# Temperature effect on redox voltage in $Li_xCo[Fe(CN)_6]_y$

Rögnvaldur Líndal Magnússon, Wataru Kobayashi, Masamitsu Takachi, and Yutaka Moritomo

Citation: AIP Advances **7**, 045002 (2017); doi: 10.1063/1.4979888
View online: http://dx.doi.org/10.1063/1.4979888
View Table of Contents: http://aip.scitation.org/toc/adv/7/4
Published by the American Institute of Physics

# Temperature effect on redox voltage in $Li_xCo[Fe(CN)_6]_y$

Rögnvaldur Líndal Magnússon,[1] Wataru Kobayashi,[1,2,3] Masamitsu Takachi,[1] and Yutaka Moritomo[1,2,3,a]
[1]*Graduate School of Pure and Applied Science, University of Tsukuba, Tsukuba 305-8571, Japan*
[2]*Faculty of Pure and Applied Science, University of Tsukuba, Tsukuba 305-8571, Japan*
[3]*Tsukuba Research Center for Interdisciplinary Materials Science (TIMS), University of Tsukuba, Tsukuba 305-8571, Japan*

(Received 3 February 2017; accepted 24 March 2017; published online 4 April 2017)

The electrochemical thermoelectric (TE) coefficient ($S_{EC} \equiv \frac{\partial V}{\partial T}$; $V$ and $T$ are the redox potential and temperature, respectively) is a significant material parameter, because it enable us to convert heat into electricity. Here, we systematically investigated the TE properties of cobalt hexacyanoferrate (Co-HCF), $Li_xCo[Fe(CN)_6]_y$, against the Li concentration ($x$). $|S_{EC}|$ is higher than the Seebeck coefficient (= 0.2 mV/K at room temperature) of $Bi_2Te_3$ and distributes from 0.2 to 0.8 mV/K. We further observed a sign reversal behavior of $S_{EC}$: $S_{EC}$ is negative at $y$ =0.71 while it is negative (positive) at $x \leq 0.3$ ($x \geq 0.6$) at $y$ =0.90. Based on the ionic model, we qualitatively reproduced the sign reversal behavior by including the volume expansion effect. These arguments suggest that $S_{EC}$ in solid is mainly governed by the electrostatic energy.  [http://dx.doi.org/10.1063/1.4979888]

Thermoelectric (TE) device, which can convert heat into electricity and vice versa, is a fascinating technology for smart society. In development of TE semiconductors, Seebeck coefficient [$S \equiv \frac{\Delta V}{\Delta T}$; $\Delta V$ ($\Delta T$) is the voltage (temperature) difference between the hot and cold electrodes] is a significant material parameter. $Bi_2Te_3$ ($S$ = 0.2 mV/K[1] at room temperature) and PbTe ( = 0.12 mV/K[2] at 300 K) are prototypical TE semiconductors and exhibit high dimensionless figure-of-merit ($ZT \equiv \frac{S^2}{\rho\kappa}T$: where $T$, $\rho$, and $\kappa$ represent temperature, resistivity, and thermal conductivity, respectively). Actually, they are in practical use for the Peltier cooling and power generation of space vehicles.[3] These materials, however, are expensive and include toxic and rare elements. In addition, these TE devices require high-grade heat source of several hundreds Kelvin to achieve 10 % -15 % of the Carnot efficiency.[4]

Recently, Kobayashi *et al.*[5] proposed a *battery-type thermocell*, whose configuration is the same as that of a lithium-ion/sodium-ion secondary batteries (LIBs/SIBs) with the exception that the anode and cathode are the same. Contrary to the conventional TE devices made by semiconductors, the battery-type thermocell converts heat into electricity through the electrochemical TE coefficient ($S_{EC} \equiv \frac{\partial V}{\partial T}$; $V$ and $T$ are the redox potential and temperature, respectively). The battery-type thermocell is low-cost and easy to fabricate, because the production processes of material and device are similar to those of LIBs. There already exists a long list of electrochemical TE effects in soluble ions/molecules,[6] *e.g.*, $[Fe(CN)_6]^{3-}/[Fe(CN)_6]^{4-}$, ($S_{EC}$ = 1.5 mV/K), $Fe^{3+}/Fe^{2+}$ ( = 0.8 mV/K), and $Cu^{2+}/Cu$ ( = 0.9 mV/K). We emphasize that the battery-type thermocell extends the usage of the electrochemical TE materials from soluble ions/molecules to insoluble solids used in LIBs/SIBs. Actually, Kobayashi *et al.*[5] fabricated CR2032-type thermocell made by layered oxides, *e.g.*, $Na_{0.99}CoO_2$ and $Na_{0.52}MnO_2$, and observed TE behavior between the anode and cathode.

[a]Corresponding author: moritomo.yutaka.gf@u.tsukuba.ac.jp

 

Transition metal hexacyanoferrates ($M$-HCF), $Li_xM[Fe(CN)_6]_y$ ($M$ is transition metal), are alternative candidates of the TE materials for the battery-type thermocell, because they show good electrochemical properties in LIBs/SIBs.[7–17] For example, thin film of $Li_{1.6}Co[Fe(CN)_6]_{0.9}2.9H_2O$ show high capacity of 132 mAh/g with good cyclability.[9] $M$-HCFs have face-centered cubic structure ($Fm\underline{3}m$: $Z = 4$). They consist of three-dimensional (3D) jungle-gym-type host framework and guest $Li^+$, which is accommodated in cubic nanopores of the framework. Importantly, the host framework, - Fe - CN - $M$ - NC - Fe -, is robust against the $Li^+$ intercalation/deintercalation and concomitant reduction/oxidization of $M$ and Fe. Actually, the host framework of $Li_{1.6}Co[Fe(CN)_6]_{0.9}2.9H_2O$ is stable even if we remove whole $Li^+$ from the framework.[9]

In this letter, we systematically investigated the TE properties of Co-HCF, $Li_xCo[Fe(CN)_6]_y$, against the Li concentration ($x$). $|S_{EC}|$ is higher than the Seebeck coefficient (= 0.2 mV/K at room temperature) of $Bi_2Te_3$ and distributes from 0.2 to 0.8 mV/K. We further observed a sign reversal behavior of $S_{EC}$ and qualitatively explained in terms of the ionic model, which include the electrostatic energy and volume expansion effect. Our observation suggests that $S_{EC}$ in solid is mainly governed by the electrostatic energy.

Thin films of $Li_xNa_{0.13}Co[Fe(CN)_6]_{0.71}$ (denoted as LCF71) and $Li_xCo[Fe(CN)_6]_{0.9}$ (LCF90) were synthesized by electrochemical deposition and following electrochemical ion exchange. First, thin films of $Na_{0.84}Co[Fe(CN)_6]_{0.71}3.6H_2O$ (NCF71) and $Na_{1.6}Co[Fe(CN)_6]_{0.90}2.9H_2O$ (NCF90) were electrochemically synthesized on an indium tin oxide (ITO) transparent electrode. Details of the synthesis conditions are described in literature.[18,19] Both the compounds shows face-centered cubic structure ($Fm\underline{3}m$: $Z = 4$) with lattice constant ($a$) of 10.3 Å (NCF71) and 10.4 Å (NCF90). The film thickness was 1.5 $\mu$m, which was determined by a profilometer (aep Technology NanoMap-LS). The ion exchange procedure was done in an Ar-filled glove box using a beaker-type cell. The cathode, anode, and electrolyte were the thin film, Li metal, and ethylene carbonate (EC)/diethyl carbonate (DEC) solution containing 1 mol/L $LiClO_4$, respectively. The charge/discharge rate was ≈ 1 C. The cut-off voltage was from 2.0 to 4.2 V. First, $Na^+$ is removed in the charge process. Then, $Li^+$ is inserted in the discharge process.

The electrochemical measurements were carried out with a potentiostat (HokutoDENKO HJ1001SD8) in an Ar-filled glove box using a beaker-type cell. The cathode, anode, and electrolyte were the thin film, Li metal, and EC/DEC containing 1 mol/L $LiClO_4$, respectively. The charge/discharge rate was ≈ 1 C. The cut-off voltage was from 2.0 to 4.2 V. The mass of each film was evaluated from thickness, area, and ideal density. $x$ in LCF71 (LCF90) was evaluated from the total current under the assumption that $x$ = 0.84 (1.6) is in the discharged state and 0.13 (0.0) is in the charged state.

Figure 1 shows prototypical example of the discharge curve of the LCF71 [(a)] and LCF90 [(b)] films. In LCF71 [Fig. 1(a)], the discharge capacity is 78 mAh/g, which is close to the ideal value (= 72 mAh/g). The curve shows a single plateau (plateau I) at ≈ 3.4 V, which is ascribed to the reduction reaction:[8] $Na_{0.13}Co^{2+}[Fe^{3+}_{0.71}Fe^{2+}_{0.29}(CN)_6]_{0.71} + 0.71Li^+ \rightarrow Li_{0.71}Na_{0.13}Co^{2+}[Fe^{2+}(CN)_6]_{0.71}$. In the discharge process, $Li^+$ is inserted into the framework, which causes the reduction of $Fe^{3+}$ to keep the charge neutrality. In LCF90 [Fig. 1(b)], the discharge capacity is 139 mAh/g, which is close

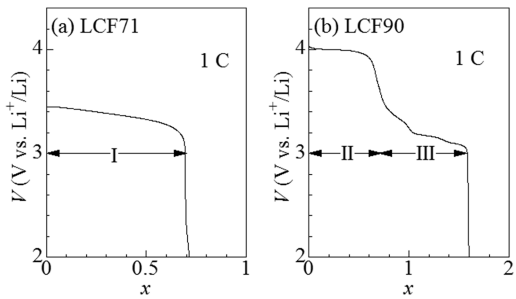


FIG. 1. Discharge curves of (a) $Li_xNa_{0.13}Co[Fe(CN)_6]_{0.71}$ (LCF71) and (b) $Li_xCo[Fe(CN)_6]_{0.9}$ (LCF90) films measured at ≈ 1 C. For convenience of explanation, we defined plateaus I, II, and III.

to the ideal value (= 132 mAh/g). The curve shows two plateaus (plateaus II and III) at ≈ 4.0 and ≈ 3.2 V. Plateau II ($x \leq 0.6$) at ≈ 4.0 V is ascribed to the reaction:[9] $Co^{3+}[Fe^{3+}_{0.6}Fe^{2+}_{0.4}(CN)_6]_{0.9} + 0.6Li^+ \rightarrow Li_{0.6}Co^{3+}[Fe^{2+}(CN)_6]_{0.9}$. Plateau III ($x \geq 0.6$) at ≈ 4.0 V is ascribed to the reaction:[8,20] $Li_{0.6}Co^{3+}[Fe^{2+}(CN)_6]_{0.9} + Li^+ \rightarrow Li_{1.6}Co^{2+}[Fe^{2+}(CN)_6]_{0.9}$. The redox potential ($V$) for $Fe^{3+}/Fe^{2+}$ is much higher in LCF90 (≈ 4.0 V; plateau II) than in LCF71 (≈ 3.4 V; plateau I). The high-$V$ is ascribed to the volume effect:[9] $a$ (≈ 9.9 Å at $x \leq 1$) of LCF90 is much smaller than $a$ (≈ 10.2 - 10.3 Å) of LCF71.[8]

Next, we carefully measured $V$ against the temperature ($T$) of the electrolyte of the battery cell. $T$ was monitored with a platinum resistance thermometer. In order to stabilize the respective $x$ state, $T$-dependent measurement was performed after the waiting time of 10 minutes. We continuously sweep the electrolyte temperature at a slow rate of ≈ 0.01 K/s. In order to minimize the temperature gradient within the cell, temperature range is set to be narrower than 7 K. Actually, $\Delta V$ [$\equiv V(T_{max})$-$V(T_{min})$, where $T_{max}$ and $T_{min}$ is the maximum and minimum temperature, respectively], slightly changes with time (≤ 1 mV) but approaches to a finite value. So, $\Delta V$ cannot be ascribed to the temperature gradient effect within the cell. The measurements was performed at every five second. Figures 2 show temperature effect on $V$ in LCF71. Red and blue marks represent data obtained in the heating and cooling runs, respectively. We evaluated $S_{EC}$ in the respective runs by least-squares fittings, as indicated by solid straight lines. Precisely speaking, we measured the temperature dependence of the difference in the potential between anode (Li) and cathode. With assuming that $S_{EC}$ of the anode (Li) is zero, we obtained $S_{EC}$ of the cathode. We observed slight drift of $V$, probably due to leak current in the battery cell, between the heating and cooling runs. At $x$ =0.16 [Fig. 2(a)], $S_{EC}$ is negative for both the heating ($S_{EC}$ = - 0.36 mV/K) and cooling (= - 0.31 mV/K) runs. Similar negative $S_{EC}$ is observed at $x$ = 0.25, 0.41, and 0.49[(b) - (d)]. Thus, we observed negative $S_{EC}$ in plateau I. Figures 3 show temperature effect on $V$ in LCF90. In plateau II ($x \leq 0.6$) region, $S_{EC}$ is negative as exemplified at $x$ = 0.21 [Fig. 3(a)]. On the other hand, in plateau III ($x \geq 0.6$) region, $S_{EC}$ is positive as exemplified at $x$ = 0.74, 0.85, and 0.96 [(b) - (d)].

We plotted in Figs. 4 the average $S_{EC}$ between the heating and cooling runs against $x$. $S_{EC}$ is negative in plateaus I and II and positive in plateau III. We note that the redox site is Fe in plateaus I and II and Co in plateau III. Thus, we observed a sign reversal behavior of $S_{EC}$ among the plateaus. In addition, $|S_{EC}|$ distributes from 0.2 mV/K to 0.8 mV/K, which are higher than the Seebeck coefficient (= 0.2 mV/K[1] at room temperature) of $Bi_2Te_3$.

Let us discuss the $x$-dependence of $S_{EC}$ in terms of a statistical thermodynamic model. In a mean-field approximation, ionic potential [$\phi(x)$] is easily calculated from the number of the $Li^+$

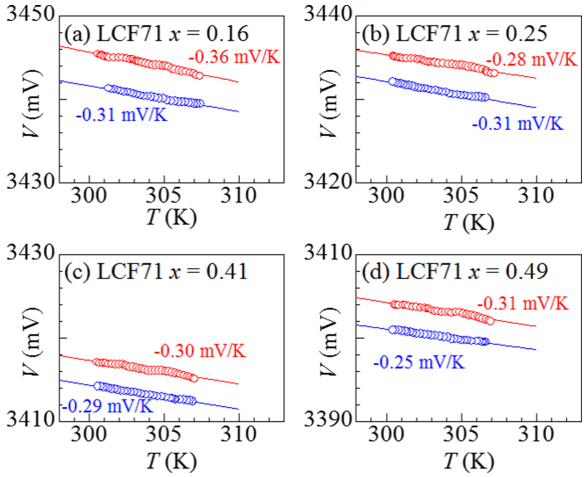


FIG. 2. Redox potential ($V$) against temperature ($T$) in LCF71: (a) $x$ = 0.16, (b) 0.25, (c) 0.41, and (d) 0.49. Red and blue marks represent data obtained in the healing and cooling runs, respectively. Solid straight lines are results of the least-squares fitting.

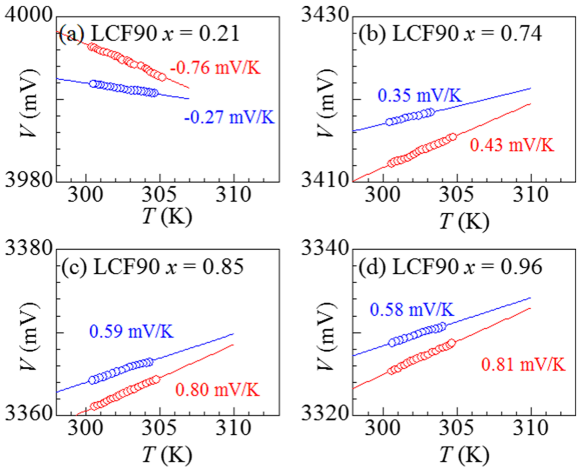


FIG. 3. Redox potential ($V$) against temperature ($T$) in LCF90: (a) $x$ = 0.21, (b) 0.74, (c) 0.85, and (d) 0.96. Red and blue marks represent data obtained in the heating and cooling runs, respectively. Solid straight lines are results of the least-squares fitting.

configurations against $x$,

$$\phi(x) = \phi_0 + k_B T \ln\left(\frac{x}{2-x}\right), \tag{1}$$

where $\phi_0$ and $k_B$ represent the site potential and the Boltzmann constant, respectively. Here, we note that number of the crystallographic $Li^+$ site is 2 per $Li_xCo[Fe(CN)_6]_y$. Taking partial differentiation with $T$, $S_{EC}$ is obtained as

$$S_{EC} = \frac{\partial V}{\partial T} = -\frac{1}{e}\frac{\partial \phi}{\partial T} = -\frac{k_B}{e}\ln\left(\frac{x}{2-x}\right). \tag{2}$$

In Figs. 4, we plotted eq. (2) as broken curves. In LCF71 [Fig. 4(b)], the occupation effect of $Na^+$ (= 0.13) is included by replacing $x$ with $x$ + 0.13. It is obvious that the statistical thermodynamic model fails to reproduce the experiment.

The ionic model,[21] which includes only $n$-th ionization energy [$I_n(M)$] of $M$, electron affinity [$A(O^-)$] of oxygen, and electrostatic energy, is known to be a good starting point to comprehend the electronic structure of transition metal compounds. Actually, Torrance *et al.*[21] have applied the model to the ground state of the transition metal oxides, and successfully reproduced the metal/insulator behavior of them. The model further quantitatively reproduced the $M$-dependences of the optical gaps in (La,Y)$MO_3$[22] and LaSr$MO_4$[23] with subtracting a constant energy of ~ 11 eV. Recently, Kobayashi *et al.*[24] applied the model to the redox potential ($V$) of Na$MO_2$ with the O3-type structure, and successfully reproduced the $M$-dependence of $V$ with subtracting a constant voltage of ~ 16.5 V.

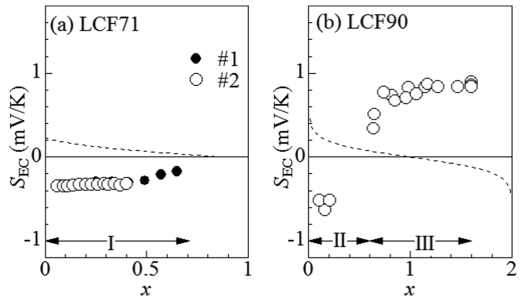


FIG. 4. Electrochemical TE coefficient ($S_{EC}$) of (a) $Li_xNa_{0.13}Co[Fe(CN)_6]_{0.71}$ (LCF71) and (b) $Li_xCo[Fe(CN)_6]_{0.9}$ (LCF90) films against $x$. Open and closed symbols in (a) represent that data were obtained from different films. Broken curves represent the calculation based on a statistical thermodynamic models (see text). I, II, and III represent the plateaus in the discharge curves.

In the ionic model, the redox potential ($V$)[24] is expressed as

$$V = \frac{1}{e}[I_3(M_r) - I_1(\mathrm{Li})] + (V_M^{M_r} - V_M^{\mathrm{Li}}) - \frac{e}{d_{M_r-\mathrm{Li}}}, \quad (3)$$

where $V_M^{M_r}$ ($V_M^{\mathrm{Li}}$), and $d_{M_r-\mathrm{Li}}$ are the Madelung potential at the redox (Li) site and the nearest-neighbor distance between the redox site and Li, respectively. Among the three terms, the first term ($\frac{1}{e}[I_3(M_M) - I_1(\mathrm{Li})]$) is essentially independent of $T$. On the other hand, the second ($V_M^{M_M} - V_M^{\mathrm{Li}}$) and third ($\frac{e}{d_{M_M-\mathrm{Li}}}$) terms should depend on $T$ through the thermal expansion effect. With putting point charges at the Co [(1/2,0,0)], Fe [(0,0,0)] and Li [(1/4,1/4,1/4)] sites (Fig. 5), we evaluated the Madelung potentials ($V_M^{\mathrm{Co}}$, $V_M^{\mathrm{Fe}}$, $V_M^{\mathrm{Li}}$) in plateaus I, II, and III. Details of the point charges ($q_{\mathrm{Co}}$, $q_{\mathrm{Fe}}$, $q_{\mathrm{Li}}$) and $x$ are listed in Table I. The Madelung potentials were calculated by the Fourier method (VESTA program[25]) at $a$ = 10.00 Å and 10.01 Å. In Table I, we also listed the Madelung potentials, the second, and third terms of eq. (3). With use of the coefficient ($\alpha$) of thermal expansion, $S_{\mathrm{EC}}$ is expressed as $S_{\mathrm{EC}} = \alpha \frac{\Delta V}{\Delta a/a}$. We tentatively used $\alpha$ (= $2.8 \times 10^{-5}$ $\mathrm{K}^{-1}$) of $Na_{1.32}Mn[Fe(CN)_6]_{0.83}3.5H_2O$, which was evaluated from Fig. 4 of Ref. 26. Then, $S_{\mathrm{EC}}$ is evaluated as -0.30 mV/K (plateau I), -0.36 mV/K (plateau II), and 0.34 mV/K (plateau III). We emphasize that the sign of the calculated $S_{\mathrm{EC}}$ in each plateau is consistent with the experiment (Fig. 4). In addition, the magnitude (= 0.3 - 0.4 mV/K) of $|S_{\mathrm{EC}}|$ is comparable to the experimental values (= 0.2 - 0.8 mV/K). Thus, the ionic model semi-qualitatively reproduces the sign reversal behavior of $S_{\mathrm{EC}}$.

In conclusion, we systematically investigated the TE properties of Co-HCF against $x$. $|S_{\mathrm{EC}}|$ is higher than the Seebeck coefficient (= 0.2 mV/K at room temperature) of $Bi_2Te_3$ and distributes from 0.2 to 0.8 mV/K. We further observed a sign reversal behavior of $S_{\mathrm{EC}}$ and qualitatively explained in terms of the ionic model, which includes the electrostatic energy and volume expansion effect. Our phenomenological approach of $S_{\mathrm{EC}}$ is easily applicable to the other materials, such as $LiMO_2$, $LiMn_2O_4$, and $LiFePO_4$, and will accelerate the material search.

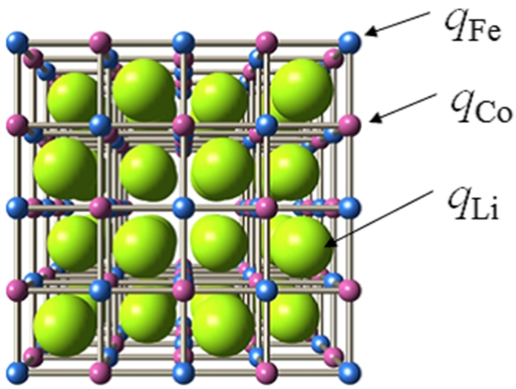


FIG. 5. Schematic structure of Co-HCF. Small blue, small red, large green spheres represent Fe, Co, and Li, respectively. Bars represent CN groups that coordinate Fe. In the Madelung calculation, we put point charges, $q_{\mathrm{Co}}$, $q_{\mathrm{Fe}}$, and $q_{\mathrm{Li}}$, at respective sites. We put the formal charge ($q_{\mathrm{Fe}}$) of the $[Fe(CN)_6]$ unit at the Fe site.

TABLE I. Point charge ($q_{\mathrm{Co}}$, $q_{\mathrm{Fe}}$, $q_{\mathrm{Li}}$), Li concentration ($x$), and Madelung potential ($V_M^{\mathrm{Co}}$, $V_M^{\mathrm{Fe}}$, $V_M^{\mathrm{Li}}$) for plateaus I, II, and III. The plateau I is for LCF71 while the plateaus II and III are for LCF90. $a$ and $x$ are the lattice constant and Li concentration, respectively. $M_r$ is the redox site.

| Plateau | $M_r$ | $a$ (Å) | $q_{\mathrm{Co}}$ | $q_{\mathrm{Fe}}$ | $q_{\mathrm{Li}}$ | $x$ | $V_M^{\mathrm{Co}}$ (V) | $V_M^{\mathrm{Fe}}$ (V) | $V_M^{\mathrm{Li}}$ (V) | $V_M^{M_r} - V_M^{\mathrm{Li}}$ (V) | $\frac{e}{d_{M_r-\mathrm{Li}}}$ (V) |
|---|---|---|---|---|---|---|---|---|---|---|---|
| I | Fe | 10.00 | + 2.0$e$ | - 3.5$e$ | + 1.0$e$ | 0.49 | -10.292 | 140.479 | -96.593 | 237.072 | 3.325 |
| I | Fe | 10.01 | + 2.0$e$ | - 3.5$e$ | + 1.0$e$ | 0.49 | -10.282 | 140.466 | -96.592 | 237.058 | 3.322 |
| II | Fe | 10.00 | + 3.0$e$ | - 3.5$e$ | + 1.0$e$ | 0.15 | -15.684 | 61.092 | -117.063 | 178.155 | 3.325 |
| II | Fe | 10.01 | + 3.0$e$ | - 3.5$e$ | + 1.0$e$ | 0.15 | -15.669 | 61.076 | -117.063 | 178.139 | 3.322 |
| III | Co | 10.00 | + 2.5$e$ | - 4.0$e$ | + 1.0$e$ | 1.10 | -12.670 | 70.202 | -59.988 | 47.317 | 3.325 |
| III | Co | 10.01 | + 2.5$e$ | - 4.0$e$ | + 1.0$e$ | 1.10 | -12.658 | 70.183 | -59.984 | 47.326 | 3.322 |

## ACKNOWLEDGMENTS

This work was supported by the Yazaki Memorial foundation for science and technology and Nippon Sheet Glass foundation for materials science and engineering. The elementary analyses were performed at the Chemical Analysis Division, Research Facility Center for Science and Engineering, University of Tsukuba.

[1] D. A. Wright, Nature **181**, 834 (1958).
[2] J. P. Heremans, V. Jovovic, E. S. Toberer, A. Saramat, K. Kurosaki, A. Charoenphakdee, S. Yamanaka, and G. J. Snyder, Science **321**, 554 (2008).
[3] H. J. Goldsmid, *Introduction to Thermoelectricity* (Springer-Verlag, Berlin, 2010).
[4] C. B. Vining, Nat. Mater. **8**, 83 (2009).
[5] W. Kobayashi, A. Kinoshita, and Y. Moritomo, Appl. Phys. Lett. **107**, 073906 (2015).
[6] I. Quickenden and Y. Mua, J. Electrochem. Soc. **142**, 3985 (1995).
[7] T. Matsuda and Y. Moritomo, Appl. Phys. Express **4**, 047101 (2011).
[8] Y. Moritomo, M. Takachi, Y. Kurihara, and T. Matsuda, Appl. Phys. Express **5**, 041801 (2012).
[9] M. Takachi, T. Matsuda, and Y. Moritomo, Jpn. J. Appl. Phys. **52**, 044301 (2013).
[10] T. Matsuda, M. Takachi, and Y. Moritomo, Chem. Commun. **49**, 2750 (2013).
[11] Y. Lu, L. Wang, J. Cheng, and J. B. Goodenough, Chem. Commun. **48**, 6544 (2012).
[12] M. Takachi, T. Matsuda, and Y. Moritomo, Appl. Phys. Express **6**, 025802 (2013).
[13] D. Yang, J. Xu, X. Z. Liao, Y. S. He, H. Liu, and Z. F. Ma, Chem. Commum. **50**, 50 (2014).
[14] H. W. Lee, R. Y. Wang, M. Pasta, S. W. Lee, N. Liu, and Y. Chi, Nat. Commun. **5**, 5280 (2014).
[15] L. Wang, J. Song, R. Qiao, L. A. Wray, M. A. Hossain, Y. D. Chung, W. Yang, Y. Lu, D. Evans, J.-J. Lee, S. Vail, X. Ahao, M. Nishijima, S. Kakimoto, and J. B. Torrance, J. Am. Chem. Soc. **137**, 2548 (2015).
[16] S. Yu, Y. Li, Y. Lu, B. Xu, Q. Wang, M. Yan, and Y. A. Jing, J. Power Sources **275**, 45 (2015).
[17] Y. You, X. L. Wu, Y. X. Yin, and Y. G. Guo, Energy Environ. Sci. **7**, 1643 (2014).
[18] F. Nakada, H. Kamioka, Y. Moritomo, J. E. Kim, and M. Takata, Phys. Rev. B **77**, 224436 (2008).
[19] K. Igarashi, F. Nakada, and Y. Moritomo, Phys. Rev. B **78**, 235106 (2008).
[20] M. Takachi and Y. Moritomo, Sci. Rep. **7**, 42694 (2017).
[21] J. B. Torrance, P. Lacorre, C. Asavaroengchai, and R. M. Metzger, Physica C **182**, 351 (1991).
[22] T. Arima, Y. Tokura, and J. B. Torrance, Phys. Rev. B **48**, 17006 (1993).
[23] Y. Moritomo, T. Arima, and Y. Tokura, J. Phys. Soc. Jpn. **64**, 4117 (1995).
[24] W. Kobayashi and Y. Moritomo, J. Phys. Soc. Jpn. **83**, 104702 (2014).
[25] K. Momma and F. Izumi, J. Appl. Crystallogr. **44**, 1272 (2011).
[26] Y. Moritomo, T. Matsuda, Y. Kurihara, and J. Kim, J. Phys. Soc. Jpn. **80**, 074608 (2011).